Featured Article

Biomechanics and clinical outcomes of various conduit configurations in valve sparing aortic root replacement

Yuanjia Zhu[1,2], Matthew H. Park[1,3], Pearly K. Pandya[1,3], Charles J. Stark[1], Danielle M. Mullis[1], Sabrina K. Walsh[1], Joo Young Kim[1], Catherine A. Wu[1], Basil M. Baccouche[1], Seung Hyun Lee[1], Abakar S. Baraka[1], Hyunchel Joo[1,4], Shin Yajima[1,5], Stefan Elde[1], Y. Joseph Woo[1,2]

[1]Department of Cardiothoracic Surgery, Stanford University, Stanford, CA, USA; [2]Department of Bioengineering, Stanford University, Stanford, CA, USA; [3]Department of Mechanical Engineering, Stanford University, Stanford, CA, USA; [4]Department of Thoracic and Cardiovascular Surgery, Yonsei University College of Medicine, Seoul, Korea; [5]Department of Cardiovascular Surgery, Osaka University Graduate School of Medicine, Osaka, Japan

Correspondence to: Y. Joseph Woo, MD. Falk Cardiovascular Research Center, Department of Cardiothoracic Surgery, Stanford University School of Medicine, Falk Bldg CV-235, 300 Pasteur Drive, Stanford, CA 94305, USA; Department of Bioengineering, Stanford University, Stanford, CA, USA. Email: joswoo@stanford.edu.

Background: Several conduit configurations, such as straight graft (SG), Valsalva graft (VG), anticommissural plication (ACP), and the Stanford modification (SMOD) technique, have been described for the valve-sparing aortic root replacement (VSARR) procedure. Prior *ex vivo* studies have evaluated the impact of conduit configurations on root biomechanics, but the mock coronary artery circuits used could not replicate the physical properties of native coronary arteries. Moreover, the individual leaflet's biomechanics, including the fluttering phenomenon, were unclear.

Methods: Porcine aortic roots with coronary arteries were explanted (n=5) and underwent VSARR using SG, VG, ACP, and SMOD for evaluation in an *ex vivo* left heart flow loop simulator. Additionally, 762 patients who underwent VSARR from 1993 through 2022 at our center were retrospectively reviewed. Analysis of variance was performed to evaluate differences between different conduit configurations, with post hoc Tukey's correction for pairwise testing.

Results: SG demonstrated lower rapid leaflet opening velocity compared with VG (P=0.001) and SMOD (P=0.045) in the left coronary cusp (LCC), lower rapid leaflet closing velocity compared with VG (P=0.04) in the right coronary cusp (RCC), and lower relative opening force compared with ACP (P=0.04) in the RCC. The flutter frequency was lower in baseline compared with VG (P=0.02) and in VG compared with ACP (P=0.03) in the LCC. Left coronary artery mean flow was higher in SG compared with SMOD (P=0.02) and ACP (P=0.05). Clinically, operations using SG compared with sinus-containing graft was associated with shorter aortic cross-clamp and cardiopulmonary bypass time (P<0.001, <0.001).

Conclusions: SG demonstrated hemodynamics and biomechanics most closely recapitulating those from the native root with significantly shorter intraoperative times compared with repair using sinus-containing graft. Future *in vivo* validation studies as well as correlation with comprehensive, comparative clinical study outcomes may provide additional invaluable insights regarding strategies to further enhance repair durability.

Keywords: Valve-sparing aortic root replacement (VSARR); biomechanics; leaflet kinematics; coronary flow; conduit configurations

Submitted May 15, 2023. Accepted for publication Jul 04, 2023. Published online Jul 28, 2023.
doi: 10.21037/acs-2023-avs2-0068
View this article at: https://dx.doi.org/10.21037/acs-2023-avs2-0068

Introduction

The valve-sparing aortic root replacement (VSARR) procedure via the remodeling technique was first proposed by Dr. Magdi Yacoub. Dr. Tirone David later described the VSARR reimplantation technique. The goal was to preserve the native aortic valve (AV) leaflets in patients with aortic root aneurysm with or without aortic regurgitation (AR) (1-4). This procedure was performed by leaving the AV and a small portion of the aortic wall attached to the left ventricular outflow tract (LVOT) and re-attaching the AV into a Dacron graft using the remodeling or reimplantation techniques (3,5). Although both techniques preserve the native AV apparatus, the remodeling technique alone does not address annular dilation and does not provide mechanical support. Therefore, results after using the remodeling technique alone have been associated with higher risks of reoperation due to AV leaflet-related pathologies and late annular dilation (6,7). Therefore, annuloplasty rings are frequently used in conjunction with the remodeling technique (6,8). The reimplantation technique, however, replaces the entire aortic root, and provides external support to the remaining abnormal valvular tissues, including the AV annulus. This may partially explain the superior outcomes observed following the reimplantation versus remodeling VSARR procedures (1,6,9).

Since the first report of the VSARR procedure, several conduit configurations have been described, namely straight graft (SG) and simple anticommissural plication (ACP) (10). The very creative Valsalva graft (VG), which is now very widely used, was first described by Dr. Ruggero De Paulis in 2000 (11). Long-term results of using the VG in VSARR were excellent (12). Under Dr. Craig Miller's leadership and pioneering innovation, the Stanford modification (SMOD) sinus-generating technique was developed and then first described in 2004 (13). All conduit configurations, with the exception of SG, focus on recreating neosinuses, as several studies demonstrated the potential role of the sinuses of Valsalva in maintaining proper flow dynamics in the aortic root through finite element modeling and patient-based four-dimensional flow images (14-20). However, these graft sinuses are generally spherical in shape, whereas the normal AV leaflets are attached to cylindrical structures with bulges in between the commissures. Furthermore, clinical studies on the utility of neosinuses vary (21,22).

Previously, our biomechanical *ex vivo* studies demonstrated that SGs, compared to sinus containing grafts, are associated with lower regurgitant fractions and leaflet opening and closing velocities (23,24). This is an important finding because the differences in leaflet velocities may have a potentially significant impact on fatigue progression, thus affecting long-term repair durability. However, previous *ex vivo* studies utilized flexible tubes as mock coronary arteries instead of native coronary arteries with buttons (23,24). Furthermore, individual leaflet biomechanics and the fluttering phenomenon were not addressed in previous studies. Therefore, in this study, we sought to comprehensively assess the impact of different conduit configurations on coronary flow and individual leaflet biomechanics using the native coronary artery tissues. A brief summary of a portion of our institution's operative experience is also presented to provide clinical perspectives on the impact of different conduit configurations on VSARR outcomes.

Methods

Experimental design

Building upon our previous *ex vivo* work, we chose to focus on SG, VG, ACP, and SMOD for this study. To minimize errors from using different samples for each conduit configurations, a repeated measures study design was adopted. Each sample in its unmodified, pre-repaired, native AV root condition served as its baseline control. Five porcine AV samples were used in this study. After baseline data collection, each sample was sequentially repaired using the VSARR procedure in different conduit configurations. After repair using each configuration, data was collected again. This resulted in five conditions measured for each valve. To minimize error due to valve decomposition and decreased tissue integrity due to repeated use of a single, unfixed porcine AV, an incomplete counterbalanced design was used where the conduit sequence was predetermined. Specifically, each conduit configuration served 1 time as the first, second, third, and final operation performed on a single valve.

Sample preparation

Complete porcine AV apparatuses (n=5) including the root and ascending aorta, along with their corresponding coronary arteries, were explanted from hearts obtained from a meat abattoir. Care was taken to preserve at least 5 mm of the LVOT tissue for mounting of the sample onto a 3D-printed elastomeric sewing ring of the aortic mount

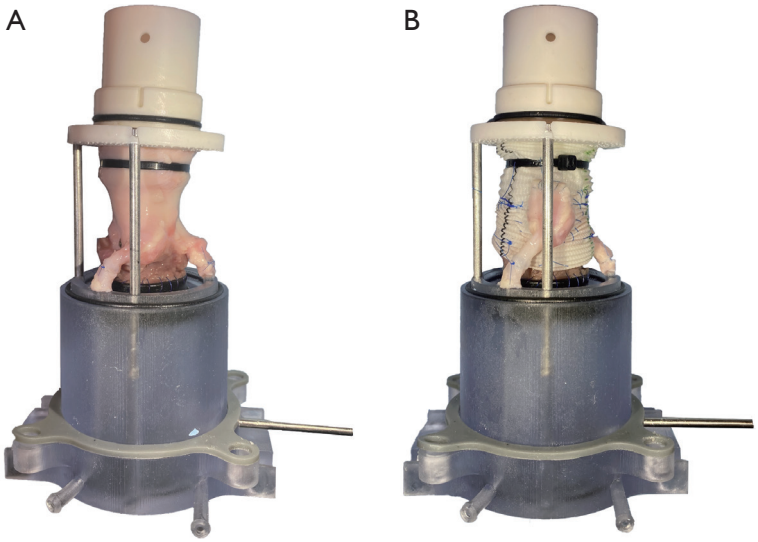

Figure 1 Aortic valve and root mounting system with native coronary arteries attached to the coronary cannulas. (A) The baseline control configuration prior to valve-sparing aortic root replacement repair; (B) the post valve-sparing aortic root replacement configuration using a straight graft.

using a running 4-0 polypropylene suture. The distal ascending aorta was affixed to the outflow mount using a cable tie. The distal coronary arteries were attached to the coronary cannulas using 6-0 polypropylene sutures (*Figure 1A*). The VSARR procedures were performed in a standard fashion based on prior published literatures and formulas published (1-4,10,12,13). Briefly, the root was dissected as low as possible to the root insertion into the ventricular muscles. The sinuses of Valsalva were resected, leaving approximately 5 mm of the aortic wall attached to the leaflet insertion sites. Generous coronary buttons were harvested. Twelve nonabsorbable 2-0 braided polyester sutures were placed from inside to outside the aorta below the leaflet insertion sites around the entire aortic annulus. Next, measurements of the AV annulus and cusp height were obtained. Conduits of the appropriate size were then selected and prepared according to published literature (1-4,10,12,13). For SG and VG configurations, the annulus sutures were loaded onto the grafts following a scalloped pattern. After sending the graft down into the root, the annulus sutures were gently tied down without decreasing the overall circumference of the graft. The commissures were then suspended and attached to the graft, ensuring proper leaflet coaptation. Lastly, 4-0 polypropylene running sutures were used to attach each AV leaflet onto the graft. For the ACP configuration, 4-0 polypropylene plication sutures were placed at the nadir of each sinus at both the annular and the sinotubular junction levels to recreate neosinuses prior to annulus suture loading onto the graft (10). For the SMOD configuration, graft 3 mm distal to the commissures were removed. A smaller graft with its diameter estimated to approximate the neosinotubular junction diameter (4) was then anastomosed onto the proximal graft using a running 4-0 polypropylene suture. Lastly, 2 ostia sites at their respective native positions were created in the graft using electrocautery. The two coronary buttons were anastomosed onto the graft using 5-0 polypropylene running sutures (*Figure 1B*). Each prepared sample was used immediately with the entire set of experiments of 5 conditions completed within 48 hours. Samples were vacuum sealed and placed in 4 ℃ overnight if not all conditions could be completed within 24 hours.

Modified aortic mounting system

The aortic mounting system was updated to allow for a streamlined coronary artery connection system (*Figure 2*). Specifically, the coronary cannulas reported previously were replaced with integrated coronary channels 3D printed into the LVOT mount. The two coronary channel inflow components had cantilevered edges designed to allow for secure placement of the native coronary arteries over the

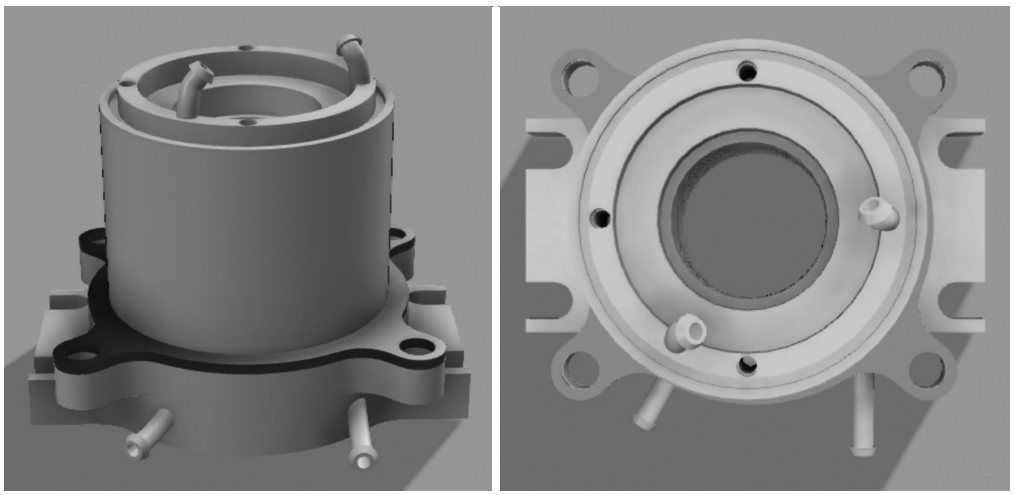

Figure 2 The updated aortic mounting system including the coronary channels through the left ventricular outflow tract mount. Note the coronary channel inflows include cantilevered edges to allow for secure attachment of the native coronary arteries to the coronary channels. The inflow angles were also designed to reflect the natural courses of the coronary arteries *in situ*.

channels using 6-0 polypropylene sutures. The angles of the coronary artery channel inflow components were designed to reflect the natural courses of the left and right coronary arteries *in situ*. The coronary artery channels then passed through the LVOT mount and exited distally. Flexible tubes then connected to the outflow channels, which then passed through a dual coronary flow circulation setup as described previously (23).

Left heart flow loop simulator

The *ex vivo* left heart flow loop simulator has been extensively described previously (23,25-30). Briefly, the *ex vivo* system consists of a linear piston pump (ViVitro Superpump, ViVitro Labs, Victoria, BC, Canada) to generate a physiologic waveform in compliance with ISO 5840 standards. Normal saline at 37 ℃ was the working fluid and was pushed from the left ventricular (LV) chamber through the AV samples, then passed compliance and resistance elements, a left atrium chamber, a calibrated disc valve, and returning back to the LV chamber. Ventricular, aortic, and left atrial pressure transducers (Utah Medical Products Inc., Midvale, UT, USA) as well as electromagnetic flow probes (Carolina Medical Electronics, East Bend, NC, USA) were used to gather pressure and flow hemodynamic data. For each sample, the pump was calibrated to generate a stroke volume of 110 mL, which with compliance and resistance adjustment and a heart rate of 70 bpm, corresponded to a mean arterial pressure of 100 mmHg for the baseline control condition. For the coronary system, the resistors were adjusted to allow for approximately 800 mL/min of coronary blood flow (31), divided into 600 mL/min for the left coronary artery and 200 mL/min for the right coronary artery (32). The compliance, resistance, and heart rate were kept the same for each sample throughout different conditions to allow for meaningful comparisons among different conduit configurations. Ten cycles of data were gathered and averaged to generate hemodynamic results. High-speed videography was also obtained via an *en face* view using a high-speed camera system that records at 1,057 frames/s with 1,280×1,024 resolution (Chronos 1.4, Kron Technologies, Burnaby, BC, Canada). Echocardiography continuous-wave doppler was acquired using a Phillips iE33 system with an S5-1 transthoracic probe (Koninklijke Philips NV, Amsterdam, The Netherlands). Analysis was performed using the iE33 on-board software and a Siemens Syngo Dynamics workstation (Siemens Medical Solutions USA, Inc., Ann Arbor, MI, USA).

Leaflet motion tracking and analysis

Leaflet motion tracking of the high-speed videography data was completed using Loggerpro3 (Vernier, Beaverton, OR, USA). Five points equally spaced apart including the Arantius nodulus were identified along the leading edge

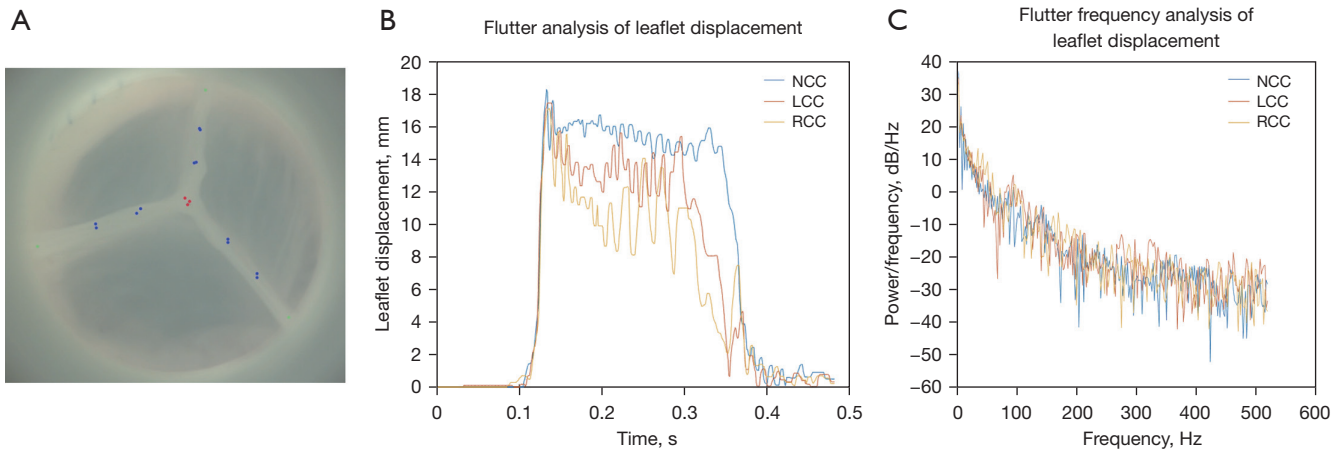

Figure 3 Leaflet motion tracking analysis demonstrating (A) 5 points equally spaced apart including the Arantius nodulus (red) that were identified along the leading edge of each leaflet for tracking. Red: Arantius nodulus of each cusp; Blue: remaining tracking points along the leading edge of each cusp. (B) A set of exemplary displacement plots were generated by converting the spatial-temporal data from the Arantius nodulus of each leaflet. (C) Flutter analyses were completed by performing Fourier transform of the displacement plots shown in (B) to identify main frequency and power. NCC, non-coronary cusp; LCC, left coronary cusp; RCC, right coronary cusp.

of each leaflet and tracked throughout a complete cardiac cycle (*Figure 3A*, *Video S1*). Data processing and analysis were performed using MATLAB (R2020a, Mathworks Inc., Natick, MA, USA). The raw spatial-temporal data was imported first and converted from pixels to international system of units. A displacement plot of each tracked point was generated (*Figure 3B*). For each displacement plot, the rapid leaflet opening and closing phases were selected and fitted using a linear regression model. The instantaneous velocities were averaged to generate the mean rapid opening and closing velocities for each tracked point. For each leaflet, 5 rapid opening and closing velocities from 5 tracked points were averaged to generate the mean leaflet velocities. In terms of relative force during leaflet rapid opening and closing, the derivatives of the velocity plots of each tracked point were calculated and averaged. This acceleration was then normalized to porcine control AVs to serve as an estimation of relative force.

To analyze the flutter phenomenon, Fourier transforms were performed and evaluated for each displacement plot, and the fundamental frequency and power were identified with their corresponding frequencies noted for each tracked point (*Figure 3C*). For each leaflet, 5 frequencies and powers calculated from the tracked points were averaged to generate the flutter frequency and power of each leaflet.

Clinical data collection

Based upon an IRB approved retrospective review of medical records, from 1993 through 2022, 762 patients who underwent VSARR at our center were identified. SG was used in 238 (32.3%) patients, ACP was used in 19 (2.6%) patients, and SMOD was used in 480 (65.1%) patients. Those who received VSARR for emergent repair of type A aortic dissection or for primarily AV repair of mixed aortic stenosis and regurgitation via pericardial leaflet augmentation, "partial Ozaki" procedures, were excluded from this analysis. The final cohort included 715 patients. Data collection was completed by retrospective chart review.

Statistical analysis

Repeated measures analysis of variance (ANOVA) and student *t*-test were performed to evaluate differences between different conduit configurations *ex vivo* and from clinical data, respectively, with *post-hoc* Tukey's correction to assess for pairwise differences. Data was analyzed using JMP Pro 17 (SAS Institute Inc., Cary, NC, USA). Statistical significance was defined at $P<0.05$ for all tests. Continuous variables were reported as mean ± standard deviation unless otherwise specified. P values shown in the tables were

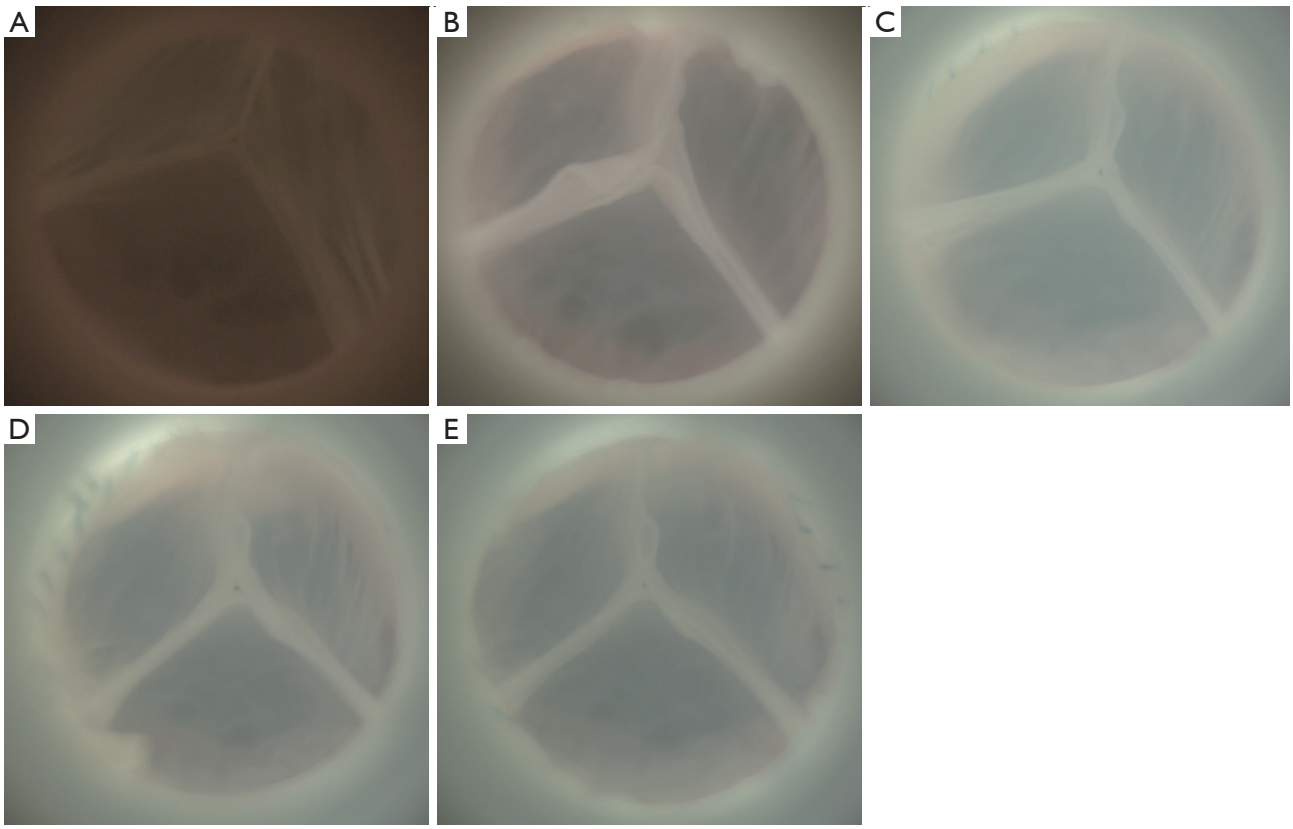

Figure 4 Exemplary en face views of the same aortic valve in diastole captured by high-speed videography for (A) baseline and after valve-sparing aortic root replacement using the (B) straight graft, (C) Valsalva graft, (D) anticommissural plication, and (E) Stanford modification conduit configurations. Notice the small central regurgitation areas in the samples prepared using the Valsalva graft, anticommissural plication, and Stanford modification conduit configurations.

calculated from repeated measures ANOVA, whereas P values reported in the text were calculated from post hoc corrections.

Results

Valve hemodynamics

Representative samples of the AV in diastole captured by high-speed videography are shown in *Figure 4*. Note the excellent AV leaflet symmetry at baseline and after VSARR repair using different conduit configurations. In samples repaired using VG, ACP, and SMOD configurations, small central regurgitant areas were consistently noticed during diastole, resulting in a small degree of valve regurgitation. Transaortic flow as well as aortic and LV pressures are shown in *Figure 5*. The SG configuration best replicated the transaortic flow tracing measured from baseline. The VG, ACP, and SMOD configurations all demonstrated flow reversal during diastole, again reflecting AV regurgitation (*Figure 5A*). Aortic leakage volume, leakage rate, and regurgitant fraction were all significantly lower in baseline compared with ACP (P=0.02, 0.03, 0.01). Aortic leakage volume and regurgitant fraction were lower in baseline compared with VG (P=0.03). Aortic regurgitant fraction was also lower in baseline compared with SMOD (P=0.03). There was no difference in aortic leakage volume, leakage rate, or regurgitant fraction between baseline and SG (P=0.42, 0.35, 0.33). Compared with SG, VG, ACP, and SMOD were associated with significantly higher aortic leakage volume (P=0.001), leakage rate (P=0.001), regurgitant fraction (P=0.001), and leakage energy loss (P=0.001, 0.001, 0.003). Aortic and LV pressure tracings

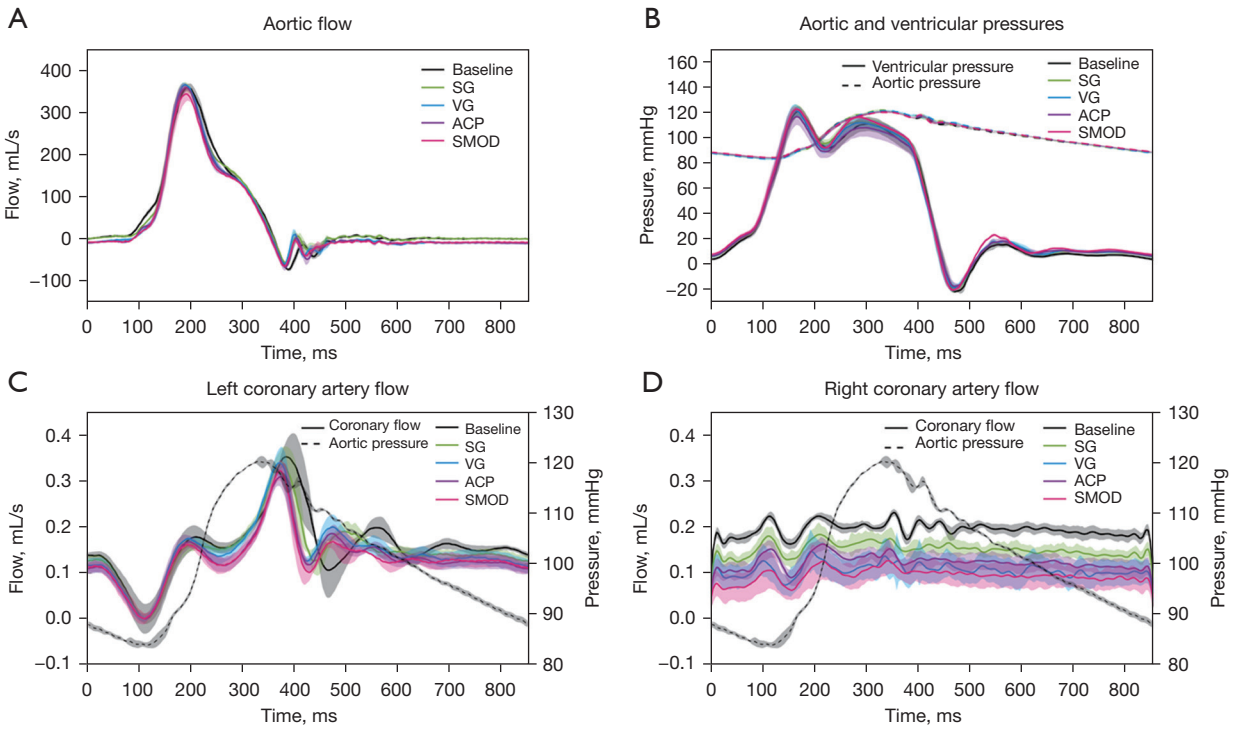

Figure 5 Aortic flow (A), aortic and ventricular pressure (B), left coronary artery flow (C) and right coronary artery flow (D) from baseline and after valve-sparing aortic root replacement repair using SG, VG, ACP, and SMOD. Notice the aortic flow reversal in diastole after repair using the VG, ACP, and SMOD configurations. The aortic flow profiles were overall similar between baseline and repair using the SG configuration. The pressure tracings were also similar among the five different conditions. No left coronary flow difference was observed across the five different conditions. VG and SMOD were associated with decreased right coronary flow compared with baseline. Black—baseline; green—SG; blue—VG; purple—ACP; red—SMOD. Solid lines in (B)—ventricular pressures; dashed lines in (B-D)—aortic pressures. Shaded areas represent standard errors. SG, straight graft; VG, Valsalva graft; ACP, anticommissural plication; SMOD, Stanford modification.

as well as transaortic pressure gradients appeared similar across different conditions (*Figure 5B*, *Table 1*). A summary of hemodynamic data is shown in *Table 1*.

Coronary hemodynamics

The left coronary artery mean flow was higher in VSARR repair using SG compared with SMOD (P=0.02) and ACP (P=0.05). The left coronary artery output was also significantly higher in VSARR repair using SG compared with VG (P=0.05) and SMOD (P=0.05). There was no difference in right coronary artery mean flow in VSARR repair using SG compared with other conduit configurations. However, the right coronary artery output was higher in VSARR repair using SG compared with VG (P=0.04) and SMOD (P=0.04). A summary of the coronary artery hemodynamics is shown in *Table 1* and *Figure 5*.

Leaflet kinematics

Representative high-speed videography footages were acquired from baseline (*Video S2*) and after VSARR repair using the SG (*Video S3*), VG (*Video S4*), ACP (*Video S5*), and SMOD (*Video S6*) configurations. Individual leaflets were tracked throughout a cardiac cycle. For the left coronary cusp (LCC), rapid opening velocity was lower in baseline compared with VG (P=0.001), ACP (P=0.02), and SMOD (P=0.006). SG also demonstrated lower rapid opening velocity compared with VG (P=0.001) and SMOD (P=0.05).

The LCC relative opening force was also lower in

Table 1 Aortic valve hemodynamics measured at baseline and after valve-sparing aortic root replacement using SG, VG, ACP, and SMOD

Variable	Baseline	SG	VG	ACP	SMOD	P value
Mean arterial pressure (mmHg)	100.0±0.1	102.1±4.0	100.9±1.3	99.9±0.6	100.4±0.2	0.36
Systolic arterial pressure (mmHg)	120.8±1.1	121.4±1.4	121.3±1.0	120.4±0.9	119.0±2.7	0.15
Diastolic arterial pressure (mmHg)	83.1±1.6	83.4±1.4	83.7±2.2	83.3±1.0	82.4±3.6	0.90
Ventricular mean pressure (mmHg)	42.9±4.5	41.4±3.4	41.7±2.5	40.1±5.7	42.3±4.5	0.94
Mean transaortic gradient (mmHg)	5.8±1.3	7.8±1.6	5.8±1.3	5.4±1.5	5.2±1.6	0.08
Pump stroke volume (mL)	110.0±0.1	110.0±0.1	110.0±0.1	110.1±0.1	110.0±0.1	0.63
Cardiac output (L/min)	3.2±0.1	3.2±0.3	3.1±0.1	3.0±0.2	2.9±0.3	0.32
Heart rate (bpm)	70.0±0.0	70.0±0.0	70.0±0.0	70.0±0.0	70.0±0.0	0.42
Aortic forward flow time (s)	0.3±0.0	0.3±0.0	0.3±0.0	0.3±0.0	0.3±0.0	0.63
Aortic forward volume (mL)	45.3±1.8	45.2±4.3	43.8±1.8	43.2±3.2	41.5±4.9	0.43
Aortic closing volume (mL)	3.1±0.7	1.6±0.3	1.5±0.3	1.9±0.3	1.9±0.3	<0.001*
Aortic leakage volume (mL)	2.3±2.4	0.7±1.3	5.3±1.6	5.6±0.2	5.0±1.1	<0.001*
Aortic leakage rate (mL/s)	4.7±4.5	1.4±2.5	9.9±2.7	10.4±0.5	9.2±1.9	<0.001*
Aortic mean flow (mL/s)	161.2±26.5	154.1±15.3	155.0±14.3	157.1±10.0	151.1±15.0	0.91
Aortic regurgitant fraction (%)	6.3±3.9	2.8±1.5	12.2±3.6	12.9±1.3	12.2±3.0	<0.001*
Aortic orifice area (cm^2)	4.5±3.3	3.8±3.5	4.0±3.4	4.2±3.2	2.8±0.9	0.91
Left coronary artery mean flow (mL/s)	0.15±0.06	0.15±0.02	0.14±0.02	0.13±0.02	0.13±0.02	0.74
Left coronary artery output (L/min)	0.64±0.10	0.68±0.16	0.55±0.22	0.51±0.23	0.70±0.26	0.20
Right coronary artery mean flow (mL/s)	0.04±0.01	0.05±0.01	0.06±0.03	0.05±0.01	0.05±0.02	0.22
Right coronary artery output (L/min)	0.15±0.06	0.20±0.10	0.07±0.04	0.08±0.05	0.22±0.24	0.21
Transaortic forward energy loss (mJ)	19.4±41.9	29.2±28.9	22.3±36.8	44.2±28.7	30.1±9.1	0.75
Transaortic closing energy loss (mJ)	14.6±8.9	4.7±1.2	4.3±1.0	6.7±1.6	5.3±1.1	0.004*
Transaortic leakage energy loss (mJ)	35.5±21.6	11.2±14.2	62.9±20.3	62.6±7.0	55.9±19.3	<0.001*
Transaortic total energy loss (mJ)	69.4±32.1	45.1±30.9	89.6±45.7	75.3±53.3	91.3±19.3	0.34

*, statistical significance. P value calculated from repeated measures analysis of variance. SG, straight graft; VG, Valsalva graft; ACP, anticommissural plication; SMOD, Stanford modification.

baseline compared with VG (P=0.001) and SMOD (P=0.05). LCC relative closing force was lower in baseline compared with VG (P=0.01) and in SG compared with VG (P=0.03). Right coronary cusp (RCC) rapid opening velocity and relative opening force were lower in baseline compared with SG (P=0.002, 0.001), VG (P=0.001), and SMOD (P=0.05). RCC rapid closing velocity was lower in SG versus VG (P=0.04). RCC relative opening force was also lower in SG compared with ACP (P=0.04). Lastly the non-coronary cusp (NCC) rapid opening velocity and relative opening force were lower in baseline compared with VG (P=0.01, 0.03). No other differences in leaflet velocity and relative force were observed.

In terms of the fluttering phenomenon, LCC flutter frequency was lower in baseline compared with VG (P=0.02) and in VG compared with ACP (P=0.03). Flutter power was lower in SG compared with ACP (P=0.01). A summary of leaflet kinematics is shown in *Table 2*.

Table 2 Aortic valve leaflet biomechanics analyzed at baseline and after valve-sparing aortic root replacement using SG, VG, ACP, and SMOD

Variable	Baseline	SG	VG	ACP	SMOD	P value
LCC rapid opening velocity (cm/s)	23.2±9.8	26.5±17.6	48.3±19.0	37.3±20.9	39.5±10.1	<0.001*
LCC rapid closing velocity (cm/s)	11.5±4.4	11.1±6.6	14.4±6.5	12.1±7.4	10.5±9.8	0.15
LCC relative opening force	1.0±0.6	1.5±1.2	2.2±1.0	1.5±1.0	1.8±0.6	0.001*
LCC relative closing force	0.6±0.5	0.6±0.4	1.1±0.9	0.7±0.5	0.8±0.5	0.01*
LCC flutter frequency (Hz)	11.9±4.1	12.9±3.8	17.7±9.7	12.2±6.8	18.5±5.6	0.01*
LCC flutter power (dB/Hz)	13.9±5.0	11.9±4.5	13.4±5.7	16.4±4.7	14.9±3.9	0.02*
RCC rapid opening velocity (cm/s)	17.2±7.0	27.7±9.8	33.1±13.1	21.2±4.8	24.9±9.9	<0.001*
RCC rapid closing velocity (cm/s)	9.0±4.3	8.1±6.2	15.0±10.6	10.9±5.8	9.2±4.0	0.04*
RCC relative opening force	1.2±0.7	3.1±1.6	3.2±1.9	1.9±1.1	2.4±1.6	<0.001*
RCC relative closing force	1.4±1.3	1.3±1.2	2.4±1.9	1.7±1.1	1.7±1.3	0.05
RCC flutter frequency (Hz)	11.2±3.8	13.4±7.8	14.1±7.0	13.9±6.1	14.3±8.9	0.52
RCC flutter power (dB/Hz)	16.6±3.4	16.9±6.0	16.7±5.4	17.0±4.4	16.3±3.8	0.99
NCC rapid opening velocity (cm/s)	6.3±3.5	12.5±13.2	18.0±20.0	11.0±6.6	11.3±8.8	0.04*
NCC rapid closing velocity (cm/s)	5.1±3.8	4.8±3.1	7.6±4.9	6.1±4.4	6.2±4.5	0.30
NCC relative opening force	1.2±0.7	2.2±1.9	2.5±2.1	1.7±1.0	1.9±1.4	0.04*
NCC relative closing force	1.0±0.8	1.0±0.7	1.7±1.1	1.3±0.9	1.2±1.1	0.07
NCC flutter frequency (Hz)	11.3±5.8	15.6±12.3	13.7±6.4	12.9±4.9	16.4±4.7	0.21
NCC flutter power (dB/Hz)	12.5±6.8	12.0±8.7	15.2±5.1	15.1±4.1	13.1±4.6	0.23

*, statistical significance. P value calculated from repeated measures analysis of variance. SG, straight graft; VG, Valsalva graft; ACP, anticommissural plication; SMOD, Stanford modification; LCC, left coronary cusp; RCC, right coronary cusp; NCC, non-coronary cusp.

Clinical outcomes

Of the 715 patients who underwent elective VSARR repair, 213 (29.8%) patients received SGs, and 502 patients (70.2%) patients received sinus containing grafts. Overall, 301 patients (42.1%) underwent concomitant procedures. Patients who received SGs were significantly older (54.4±1.0 years) compared with those that received sinus containing grafts (41.8±14.6 years, P<0.001). Average aortic cross-clamp times for SG and sinus containing graft were 155.2±53.1 and 234.9±100.6 minutes, respectively (P<0.001). Average cardiopulmonary bypass times for SG and sinus containing graft were 199.5±70.1 and 296.0± 64.3 minutes, respectively (P<0.001). Average hospital length of stay after VSARR using the SG and sinus containing graft were 8.3±0.3 and 8.0±4.4 days (P=0.47). Postoperatively, extracorporeal membrane oxygenation was used in 1 (0.5%) patient who received SG and 3 (0.7%) patients who received sinus containing graft (P=0.72). The 30-day, 1-year, and overall mortality rate using SG and sinus containing graft were 0 (0%) and 1 (0.2%); 3 (1.4%) and 2 (0.4%); 5 (2.3%) and 17 (3.5%), respectively.

Discussion

In this study, we used native coronary arteries to simulate VSARR repair using four different conduit configurations. Similar to our previous *ex vivo* evaluation of the VSARR operation, we again confirmed that SG, compared with sinus containing graft, most closely recapitulated the native aortic root biomechanics (23). Given that a multitude of studies demonstrated the impact of sinuses of Valsalva on AV cusp kinematics, coronary blood flow, and hemodynamics (33-35), results from this highly clinically relevant *ex vivo* study may provide additional important insight for this operation.

The results from this study were largely consistent with

what have been reported previously (23). Clinically, we observed the use of SG was associated with over 60 fewer minutes of aortic cross-clamp time compared with using sinus containing graft. We hypothesized that the difference in intraoperative time was due to the simplicity of SG implantation without the need to recreate neosinuses or operate within the spherically shaped root, which could be technically challenging. The use of the SG configuration is very straightforward, easy to adopt, and does not require additional modifications or anastomosis. We also found that postoperative outcomes were similar between the two conduit configurations. The SG is generally widely available throughout the world from multiple manufacturers and is lower in cost compared with other options using grafts with neosinuses or multiple grafts. These factors make the SG a valuable conduit for the VSARR operation. The advances in leaflet kinematics analysis and coronary flow measurement technology enhance the validity and accuracy of *ex vivo* AV simulation by incorporating native coronary artery tissues in our biomechanical experiments. The inclusion of coronary buttons and the physical properties of the native tissues allowed for a more accurate assessment of the VSARR procedure in the *ex vivo* system. We observed that all conduit configurations, except for SG, were associated with some degree of mild AR. This may be because for both ACP and SMOD, oversized grafts were used (10,13). The oversizing was proposed with the intention to generate a neosinus. However, this significantly increases the neo aortic root diameter. The AV commissures, therefore, are externally, radially displaced. This displacement in commissure positions can have significant impact on leaflet coaptation and geometry (30).

In terms of leaflet kinematics, SG consistently appeared to demonstrate similar leaflet velocities, relative force, and fluttering compared with the native AV root. We hypothesized that in the sinus containing graft configurations, radial AV commissure displacement likely influenced cusp velocities and relative forces because of a greater leaflet travel distance within the same amount of time in each cardiac cycle. Leaflet fluttering, though, did not appear to differ greatly across different configurations. SG, ACP, and SMOD all demonstrated similar flutter frequencies compared with baseline. Though previous literature demonstrated the importance of neosinuses in leaflet biomechanics and flow dynamics in the aortic root (36,37), our findings suggest that a near normal leaflet biomechanics can be achieved using SG. We believe that the generous coronary buttons that were used and attached to the aortic root may provide the SG similarity in reconstituting the healthy, physiologic dynamics. Given that increased leaflet fluttering, opening and closing velocities, and forces may contribute to additional mechanical cyclic loading on the leaflets during systole (38), which can influence early structural valve failure (39), the findings from our study may provide important information to help improve long-term repair durability.

Significantly higher coronary artery mean flow was observed in SG compared with ACP and SMOD in the left coronary artery. The overall coronary output was higher in SG compared with sinus containing graft configurations. This is an important finding because studies have also shown that coronary flow can impact AV leaflet biomechanics and sinus hemodynamics (40). However, the flow dynamics in the root may also impact coronary flow, and further investigations may be warranted to further address this question. Though the absolute quantitative measurements may not appear to be clinically significant, the impact of this difference on leaflet biomechanics could have a much greater effect on repair durability.

Given the *ex vivo* experimentation system and the retrospective nature of the clinical arm of this study, limitations exist. Porcine hearts have been widely adopted for simulation work due to their high degree of similarity with human hearts in terms of anatomy and relative size. However, small differences still exist in leaflet thickness and individual leaflet sizes (23,25,27,29,30). These differences may influence the root biomechanics. Human samples may be used as the immediate next step to further validate our *ex vivo* findings, and large animal *in vivo* studies may be carried out to account for the differences between the *in vivo* environment and the *ex vivo* setup. Next, normal saline was used in the simulator to allow proper functioning of the magnetic flow probes. However, the viscosity difference between saline and blood may lead to differences in small-scale turbulent flow (23). Lastly, the clinical data summarized in this study were obtained from a descriptive analysis. Therefore, a comprehensive, comparative analysis will need to be performed to more closely evaluate our center's clinical experience in VSARR using different conduit configurations.

Acknowledgments

Funding: We would like to thank the generous donation from the Rittenberg Family Foundation that made this work possible. This work was also supported by the National

Institutes of Health (NIH R01 HL152155, YJW; NIH F32 HL158151, YZ), the Thoracic Surgery Foundation Resident Research Fellowship (YZ), the Japan Heart Foundation (SY), and the American Heart Association (PKP). The content is solely the responsibility of the authors and does not necessarily represent the official views of the funders.

Footnote

Conflicts of Interest: The authors have no conflicts of interest to declare.

References

1. David TE, Feindel CM, Webb GD, et al. Long-term results of aortic valve-sparing operations for aortic root aneurysm. J Thorac Cardiovasc Surg 2006;132:347-54.
2. David TE. Remodeling the aortic root and preservation of the native aortic valve. Operative Techniques 1996;1:44-56.
3. David TE, Feindel CM, Bos J. Repair of the aortic valve in patients with aortic insufficiency and aortic root aneurysm. J Thorac Cardiovasc Surg 1995;109:345-51; discussion 351-2.
4. David TE, Feindel CM. An aortic valve-sparing operation for patients with aortic incompetence and aneurysm of the ascending aorta. J Thorac Cardiovasc Surg 1992;103:617-21; discussion 622.
5. Zhu Y, Woo YJ. Cusp repair techniques in bicuspid and tricuspid aortic valves. JTCVS Tech 2021;7:109-16.
6. Chauvette V, Kluin J, de Kerchove L, et al. Outcomes of valve-sparing surgery in heritable aortic disorders: results from the AVIATOR registry. Eur J Cardiothorac Surg 2022;62:ezac366.
7. Giebels C, Fister JC, Ehrlich T, et al. Failures of Valve-sparing Aortic Root Replacement Using the Root Remodeling Technique. Ann Thorac Surg 2022;113:2000-6.
8. Lenoir M, Maesen B, Stevens LM, et al. Reimplantation versus remodelling with ring annuloplasty: comparison of mid-term outcomes after valve-sparing aortic root replacement. Eur J Cardiothorac Surg 2018;54:48-54.
9. Liu L, Wang W, Wang X, et al. Reimplantation versus remodeling: a meta-analysis. J Card Surg 2011;26:82-7.
10. Gleason TG. New graft formulation and modification of the David reimplantation technique. J Thorac Cardiovasc Surg 2005;130:601-3.
11. De Paulis R, De Matteis GM, Nardi P, et al. A new aortic Dacron conduit for surgical treatment of aortic root pathology. Ital Heart J 2000;1:457-63.
12. De Paulis R, Scaffa R, Nardella S, et al. Use of the Valsalva graft and long-term follow-up. J Thorac Cardiovasc Surg 2010;140:S23-7; discussion S45-51.
13. Demers P, Miller DC. Simple modification of "T. David-V" valve-sparing aortic root replacement to create graft pseudosinuses. Ann Thorac Surg 2004;78:1479-81.
14. Grande-Allen KJ, Cochran RP, Reinhall PG, et al. Re-creation of sinuses is important for sparing the aortic valve: a finite element study. J Thorac Cardiovasc Surg 2000;119:753-63.
15. Bellhouse BJ, Bellhouse FH, Reid KG. Fluid mechanics of the aortic root with application to coronary flow. Nature 1968;219:1059-61.
16. Kvitting JP, Ebbers T, Wigström L, et al. Flow patterns in the aortic root and the aorta studied with time-resolved, 3-dimensional, phase-contrast magnetic resonance imaging: implications for aortic valve-sparing surgery. J Thorac Cardiovasc Surg 2004;127:1602-7.
17. Gaudino M, Piatti F, Lau C, et al. Aortic flow after valve sparing root replacement with or without neosinuses reconstruction. J Thorac Cardiovasc Surg 2019;157:455-65.
18. Galea N, Piatti F, Lau C, et al. 4D flow characterization of aortic blood flow after valve sparing root reimplantation procedure. J Vis Surg 2018;4:95.
19. Galea N, Piatti F, Sturla F, et al. Novel insights by 4D Flow imaging on aortic flow physiology after valve-sparing root replacement with or without neosinuses. Interact Cardiovasc Thorac Surg 2018;26:957-64.
20. Salica A, Pisani G, Morbiducci U, et al. The combined role of sinuses of Valsalva and flow pulsatility improves energy loss of the aortic valve. Eur J Cardiothorac Surg 2016;49:1222-7.
21. Beckmann E, Leone A, Martens A, et al. Comparison of Two Strategies for Aortic Valve-Sparing Root Replacement. Ann Thorac Surg 2020;109:505-11.
22. David T. Reimplantation valve-sparing aortic root replacement is the most durable approach to facilitate

aortic valve repair. JTCVS Tech 2021;7:72-8.
23. Paulsen MJ, Imbrie-Moore AM, Baiocchi M, et al. Comprehensive Ex Vivo Comparison of 5 Clinically Used Conduit Configurations for Valve-Sparing Aortic Root Replacement Using a 3-Dimensional-Printed Heart Simulator. Circulation 2020;142:1361-73.
24. Paulsen MJ, Kasinpila P, Imbrie-Moore AM, et al. Modeling conduit choice for valve-sparing aortic root replacement on biomechanics with a 3-dimensional-printed heart simulator. J Thorac Cardiovasc Surg 2019;158:392-403.
25. Zhu Y, Imbrie-Moore AM, Park MH, et al. Ex Vivo Analysis of a Porcine Bicuspid Aortic Valve and Aneurysm Disease Model. Ann Thorac Surg 2021;111:e113-5.
26. Zhu Y, Marin-Cuartas M, Park MH, et al. Ex vivo biomechanical analysis of the Ross procedure using the modified inclusion technique in a 3-dimensionally printed left heart simulator. J Thorac Cardiovasc Surg 2021;S0022-5223(21)01315-5.
27. Zhu Y, Imbrie-Moore AM, Paulsen MJ, et al. Novel bicuspid aortic valve model with aortic regurgitation for hemodynamic status analysis using an ex vivo simulator. J Thorac Cardiovasc Surg 2022;163:e161-71.
28. Zhu Y, Wilkerson RJ, Pandya PK, et al. Biomechanical Engineering Analysis of Pulmonary Valve Leaflet Hemodynamics and Kinematics in the Ross Procedure. J Biomech Eng 2023;145:011005.
29. Zhu Y, Imbrie-Moore AM, Paulsen MJ, et al. A Novel Aortic Regurgitation Model from Cusp Prolapse with Hemodynamic Validation Using an Ex Vivo Left Heart Simulator. J Cardiovasc Transl Res 2021;14:283-9.
30. Zhu Y, Park MH, Imbrie-Moore A, et al. Biomechanical evaluation of aortic regurgitation from cusp prolapse using an ex vivo 3D-printed commissure geometric alignment device. J Cardiothorac Surg 2022;17:303.
31. Ramanathan T, Skinner H. Coronary blood flow. Contin Educ Anaesth Crit Care Pain 2005;5:61-64. doi:10.1093/BJACEACCP/MKI012
32. Goodwill AG, Dick GM, Kiel AM, et al. Regulation of Coronary Blood Flow. Compr Physiol 2017;7:321-82.
33. Miller DC. Rationale and results of the Stanford modification of the David V reimplantation technique for valve-sparing aortic root replacement. J Thorac Cardiovasc Surg 2015;149:112-4.
34. De Paulis R, Chirichilli I, Scaffa R, et al. Long-term results of the valve reimplantation technique using a graft with sinuses. J Thorac Cardiovasc Surg 2016;151:112-9.
35. Gaudino M, Weltert L, Munjal M, et al. Early clinical outcome after aortic root replacement using a biological composite valved graft with and without neo-sinuses. Eur J Cardiothorac Surg 2017;51:316-21.
36. Leyh RG, Schmidtke C, Sievers HH, et al. Opening and closing characteristics of the aortic valve after different types of valve-preserving surgery. Circulation 1999;100:2153-60.
37. Katayama S, Umetani N, Sugiura S, et al. The sinus of Valsalva relieves abnormal stress on aortic valve leaflets by facilitating smooth closure. J Thorac Cardiovasc Surg 2008;136:1528-35, 1535.e1.
38. Vennemann B, Rösgen T, Heinisch PP, et al. Leaflet Kinematics of Mechanical and Bioprosthetic Aortic Valve Prostheses. ASAIO J 2018;64:651-61.
39. Avelar AHF, Canestri JA, Bim C, et al. Quantification and Analysis of Leaflet Flutter on Biological Prosthetic Cardiac Valves. Artif Organs 2017;41:835-44.
40. Moore BL, Dasi LP. Coronary Flow Impacts Aortic Leaflet Mechanics and Aortic Sinus Hemodynamics. Ann Biomed Eng 2015;43:2231-41.

Cite this article as: Zhu Y, Park MH, Pandya PK, Stark CJ, Mullis DM, Walsh SK, Kim JY, Wu CA, Baccouche BM, Lee SH, Baraka AS, Joo H, Yajima S, Elde S, Woo YJ. Biomechanics and clinical outcomes of various conduit configurations in valve sparing aortic root replacement. Ann Cardiothorac Surg 2023;12(4):326-337. doi: 10.21037/acs-2023-avs2-0068

